Nano Res (2010) 3: 1–7
DOI 10.1007/s12274-010-1001-9
Research Article

Shape Control of CoO and $LiCoO_2$ Nanocrystals

Dingsheng Wang[1], Xiaoling Ma[1], Yanggang Wang[1], Li Wang[2], Zhongying Wang[1], Wen Zheng[1], Xiangming He[2], Jun Li[1], Qing Peng[1], and Yadong Li[1] (✉)

[1] Department of Chemistry and State Key Laboratory of New Ceramics and Fine Processing, Tsinghua University, Beijing 100084, China
[2] Institute of Nuclear and New Energy Technology, Tsinghua University, Beijing 102201, China

Received: 15 September 2009 / Revised: 10 October 2009 / Accepted: 9 November 2009

ABSTRACT

Shape control of nanocrystals has become a significant subject in materials science. In this work, we describe a convenient way to achieve morphology-controllable synthesis of CoO nanocrystals including octahedrons and spheres as well as $LiCoO_2$ polyhedrons and spheres. In particular, we explain the formation of CoO octahedrons exposing only high-energy (111) facets using theoretical calculations; these should also be a useful tool for directing future face-controlled preparation of other nanocrystals. More importantly, the as-obtained $LiCoO_2$ nanocrystals showed different electrochemical performance depending on their morphology, indicating that Li-insertion/deintercalation dynamics might be crystal face-sensitive.

KEYWORDS

CoO, $LiCoO_2$, nanocrystals, lithium-ion batteries

Introduction

Morphology-controllable synthesis of nanocrystals is very important because there is a significant relationship between crystal morphology (exposing well-defined crystal facets) and intrinsic chemical and physical properties [1–5]. From a theoretical perspective, it is essential to explore the decisive parameters influencing the final crystal morphology in order to deeply understand the growth kinetics and structural polymorphism in nanocrystals [6–10]; from a practical perspective, it is necessary to develop effective synthetic strategies modifying the crystal morphology in order to design and fabricate nanomaterials with optimized crystal facets exhibiting tailored properties [11–14].

CoO nanocrystals have attracted a tremendous amount of attention from researchers due to their electrochemical, magnetic, and catalytic properties and the corresponding potential applications in battery materials, magnetic data storage, and catalysis [15–18]. In particular, the lithium-containing compound, $LiCoO_2$, is the most attractive lithium battery material owing to it having the best performance in terms of high specific energy density and excellent cycle life [19–22].

CoO nanocrystals with various sizes and morphologies have been synthesized via several chemical synthetic procedures [23–27], including the thermal decomposition of organometallic compounds such as $Co_2(CO)_8$ [28], Co(II) cupferronate [29], and $Co(acac)_3$ (acac = acetylacetonate) [30] or metal-oleate complexes [31]. There have been fewer reports of $LiCoO_2$ nanocrystals with well-defined crystal morphologies due to the synthetic difficulties involved in preparing

Address correspondence to ydli@mail.tsinghua.edu.cn

such materials [32]. Herein, we describe a convenient way to achieve morphology-controllable synthesis of CoO nanocrystals including octahedrons and spheres using $Co(NO_3)_2 \cdot 6H_2O$ as a precursor. Then, using the as-prepared CoO nanocrystals as a cobalt source and $LiOH \cdot H_2O$ as a lithium source, $LiCoO_2$ nanocrystals were synthesized via a simple solid-state reaction. On lithium intercalation, the CoO octahedrons evolved into $LiCoO_2$ polyhedral nanostructures, while the spheres retained the original nanostructured morphology. The differences in electrochemical properties between the two kinds of novel-shaped $LiCoO_2$ nanocrystals were investigated.

1. Experimental

Materials. All reagents, including $Co(NO_3)_2 \cdot 6H_2O$, $LiOH \cdot H_2O$, octadecylamine (ODA), oleic acid (OA), ethanol, and cyclohexane, were of analytical grade and obtained from the Beijing Chemical Factory, China. They were used without further purification.

Synthesis of CoO octahedrons. In a typical synthesis of CoO octahedra, 10 g of $Co(NO_3)_2 \cdot 6H_2O$ was added to 50 mL of ODA at 250–280 °C (10 g of $Co(NO_3)_2 \cdot 6H_2O$ cannot be completely dissolved in 50 mL of ODA solvent). After the reaction was complete (within 30 min), the final products were collected and washed several times with ethanol.

Synthesis of CoO spheres. The preparation was carried out as above, except that 20 mL of OA were added to the 50 mL of ODA.

Synthesis of $LiCoO_2$ nanocrystals. 1 g of as-prepared CoO nanocrystals and 0.56 g of $LiOH \cdot H_2O$ were mixed and calcined in air at 500 °C for 30 min.

Characterization. Powder X-ray diffraction patterns were recorded with a Bruker D8 Advance X-ray powder diffractometer with Cu Kα radiation (λ = 1.5406 Å). The morphology of as-synthesized samples was determined by using a Hitachi model H-800 transmission electron microscope, a JEOL JSM-6301F scanning electron microscope, and a JEOL 2010F high-resolution transmission electron microscope.

Computational details. Calculations were carried out using the DMol3 Program (version 4.0). To describe the valence orbitals of the atoms, the double numerical plus polarization (DNP) basis set was used in the calculations. The effective core potentials (ECP) method was adopted for core treatment. The density functional theory (DFT) study was performed with a generalized-gradient approximation (GGA) using the Perdew–Burke–Ernzerhof (PBE) functional. In each calculation, stoichiometric slab models were used. To be consistent with the experimental work in this paper, the clean (001) and (111) surfaces both consisted of four atomic layers and a total of 32 atoms, while the clean (001) surface included eight atomic layers and a total of 32 atoms. Each of these surfaces contains 16 Co atoms and 16 O atoms. We used an 8 k × 8 k × 8 k point mesh for the bulk crystal and an 8 k × 8 k × 1 k point mesh for the slabs. The calculated lattice constant is 4.195 Å, close to the experimental value of 4.266 Å. The slabs were repeated periodically with a vacuum spacing of 15 Å. The two top layers of the substrate were allowed to relax and all other layers were kept fixed in all geometry optimizations. In the geometry optimizations the total energy was converged to 0.002 eV.

Electrochemical measurements. Charge / discharge tests were carried out using coin-type cells (size: 2016), which consisted of an active material working electrode and a Li foil counter electrode separated by a Celgard 2300 microporous membrane. The electrode was prepared by mixing the active material with 15 wt% acetylene black and 5 wt% polytetrafluroethylene (PTFE) binder, and compressing the mixture onto an aluminum mesh current collector. The area of the mixture was 0.785 cm^2. Typical loadings of the electrodes were between 6 and 7 mg/cm^2 of active material. A 1 mol/L solution of $LiPF_6$ dissolved in ethylene carbonate/dimethyl carbonate (EC/DMC) (1:1 volume ratio) was used as the electrolyte. The cells were assembled in an argon-filled glove box (Mikrouna, Super 1220/7 50, China).

2. Results and discussion

In our synthesis of CoO nanocrystals, $Co(NO_3)_2 \cdot 6H_2O$ was used as the starting material while ODA and OA

were used as both solvent and surfactant. The reaction was performed in air and was complete within 30 min. About 2 g of products could be prepared in a one-pot synthesis. Figure 1 shows scanning electron microscope (SEM), transmission electron microscope (TEM), and high-resolution TEM (HRTEM) images of as-obtained samples. It can be seen that CoO nanocrystals with a uniform morphology consisting of octahedrons (Fig. 1(a)) or spheres (Fig. 1(d)) can be synthesized in monosurfactant (ODA) and mixed surfactant (ODA and OA) systems, respectively. Selected area electron diffraction (SAED) patterns indicate that there is a great difference between these two samples. The CoO octahedrons are perfectly monocrystalline (Fig. 1(b), inset) while the spheres (Fig. 1(e), inset) are not. The HRTEM images of individual nanocrystals confirm this difference. From Fig. 1(c), we can see that the CoO octahedrons crystallize with no obvious defects or dislocations. However, Fig. 1(f) illustrates that the CoO spheres are composed of aggregates of smaller nanoparticles. Powder X-ray diffraction (XRD) experiments were carried out to further determine the structure and composition of the as-prepared products. The series of Bragg reflections in the patterns (see Electronic Supplementary Material (ESM), Fig. S-1) correspond to cubic phase CoO (JCPDS 48-1719). For the CoO spheres, the relative intensities of the diffraction peaks are the same as those in the standard pattern. In contrast, in the pattern of the CoO octahedra, the intensity of the (111) peak is significantly larger than that of the (200) peak, indicating that the CoO octahedrons have exposed (111) facets.

In order to understand the formation of (111)-predominant nanocystals, we analyzed the energy relationship between different crystallographic facets of CoO in the ODA system using theoretical calculations. To simplify the calculation process,

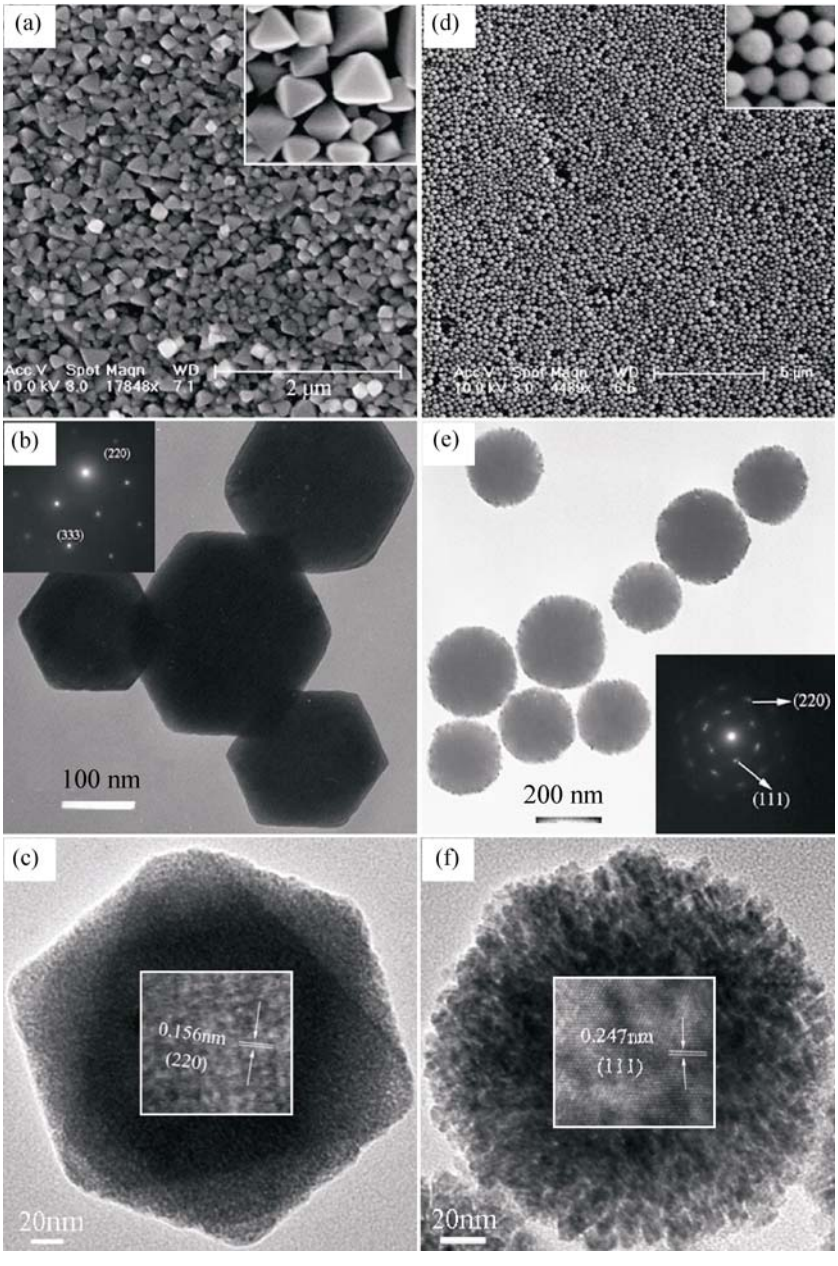

Figure 1 (a) and (d) SEM images of CoO octahedrons and spheres, respectively. (b) and (e) TEM images and corresponding SAED patterns (insets) of these two samples. (c) and (f) HRTEM images of individual nanocrystals of these two samples

methylamine was used as a simple model molecule to investigate the binding behavior of ODA adsorbed on CoO surfaces (this is reasonable because this binding mainly comes from the interaction between the lone pair of electrons in the $-NH_2$ functional group and the unoccupied d orbitals in Co^{2+} ions). Figure 2 illustrates models of methylamine adsorbed on (001), (011), and (111) surfaces. The surface energy was obtained from the difference between the lattice energy of the specified slab model and that of the same number of CoO units in the bulk state [33]. The adsorption energy was calculated using Eq. (1):

$$E_{\text{adsorption}} = -(E_{\text{surface+adsorbate}} - E_{\text{surface}} - E_{\text{adsorbate}}) \quad (1)$$

where $E_{\text{surface+adsorbate}}$ is the energy of the adsorption complex including the relaxed surface and adsorbate molecule, E_{surface} is the energy of the isolated surface, and $E_{\text{adsorbate}}$ is the energy of the isolated adsorbate molecule. The computational details are given in the Experimental section and the results are shown in Table 1. From the calculation results, we can see that, for cubic CoO, the (111) facets are the surfaces with the highest energy, which means that they usually diminish rapidly during the crystal growth process as a result of the minimization of surface energy. However, in the ODA system, CoO nanocrystals exposing only (111) facets can be obtained because the interactions between ODA and various facets are different. The interaction between ODA and (111) facets is much stronger than those between ODA and other facets, leading to the protection of (111) facets by the adsorbed ODA surfactant and subsequent crystal evolution to a shape whose exposed facets are all (111) ones.

Table 1 Surface energy and adsorption energy of CH_3NH_2 on each surface of CoO

Surface index	(100)	(110)	(111)
Surface energy (J/m^2)	1.666	2.565	5.845
Adsorption energy (eV)	0.775	0.749	1.110
Bond length of Co–N (Å)	2.010	1.991	2.095

On the other hand, when OA was added to the reaction system, the as-obtained products had a spherical morphology instead of octahedral. Each CoO sphere is composed of smaller particles, so they have no predominant facets. The reason might be that the interaction between OA and CoO crystals is stronger than that between ODA and CoO crystals. The strong adsorption of OA on CoO surface handicaps the growth of CoO crystals, leading to the formation of small particles. However, the mechanism of formation of the CoO spheres is not very clear and further investigation is needed.

Generally, nanocrystals are more reactive than their bulk counterparts due to their smaller size. So, using CoO nanocrystals as precursors instead of commercial cobalt salts to produce $LiCoO_2$ might overcome the difficulties in preparing $LiCoO_2$ nanocrystals. Indeed, we can successfully synthesize $LiCoO_2$ nanocrystals by a simple solid-state reaction between as-obtained CoO nanocrystals and a lithium source such as $LiOH{\cdot}H_2O$ at low temperature (500 ˚C) within a short time (30 min). The reaction was performed in air and can be depicted as follows:

$$4\text{CoO(nanocrystals)} + 4\text{LiOH} + \text{O}_2 \longrightarrow 4\text{LiCoO}_2\text{(nanocrystals)} + 2\text{H}_2\text{O} \quad (2)$$

The composition of the as-obtained products was examined by XRD (see Fig. S-2 in the ESM). The patterns in Fig. S-2 are in good agreement with the standard pattern for $LiCoO_2$ (JCPDS 44-0145). Interestingly, novel-shaped $LiCoO_2$ nanocrystals resulted from this process. When CoO

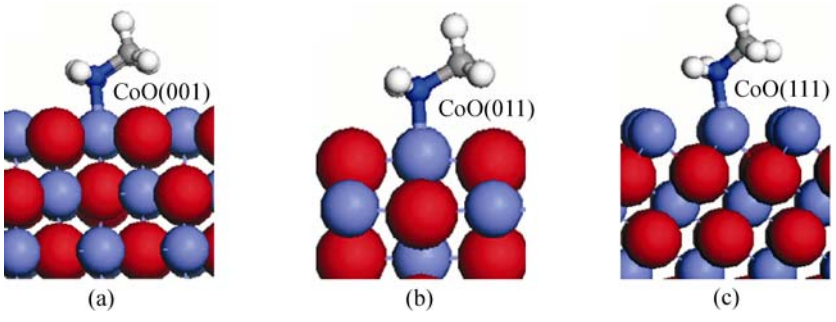

Figure 2 Adsorption of methylamine on each surface of CoO: (a) CoO(001), (b) CoO(011), and (c) CoO(111). Red spheres: oxygen; Cambridge blue spheres: cobalt; white spheres: hydrogen; navy blue spheres: nitrogen; grey spheres: carbon

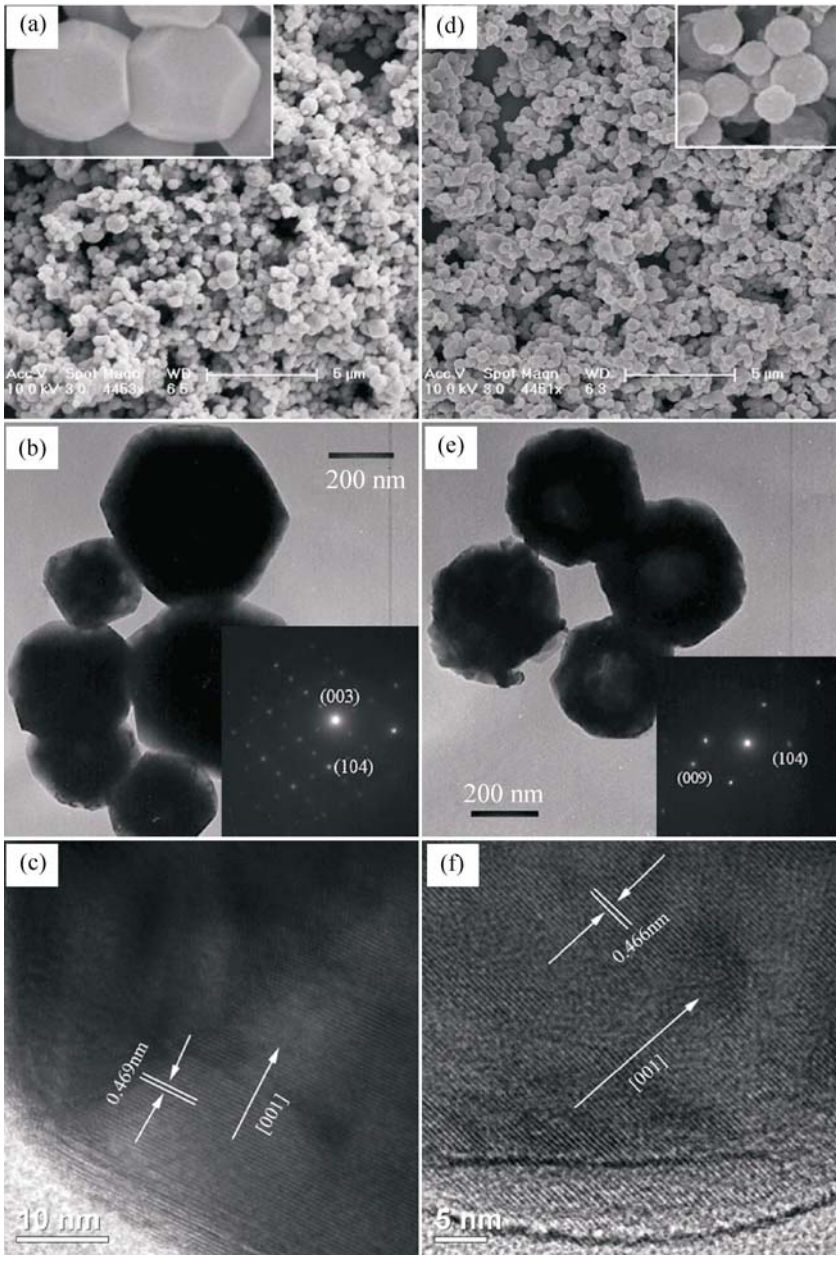

Figure 3 (a) and (d) SEM images of $LiCoO_2$ polyhedrons and spheres, respectively. (b) and (e) TEM images and corresponding SAED patterns (insets) of these two samples. (c) and (f) HRTEM images of nanocrystals of these two samples

octahedrons were used as the cobalt source, $LiCoO_2$ polyhedrons were obtained, while the CoO spheres retained their spherical morphology when reacting with the lithium source. Figure 3 shows SEM and TEM images of the $LiCoO_2$ nanocrystals. From the high-resolution images (Figs. 3(a) and 3(d), insets), polyhedral and spherical nanostructures of $LiCoO_2$ can be clearly observed. The SAED patterns (Figs. 3(b) and 3(e), insets) indicate that both the samples are well-crystallized. Figures 3(c) and 3(f) reveal clear lattice fringes with interplanar distances of about 0.469 and 0.466 nm, respectively, which correspond to the (003) planes in bulk $LiCoO_2$.

The crystal morphology of nanocrystals can greatly influence their properties. Recently, much endeavor has focused on the synthesis of novel-shaped lithium battery materials and investigation of the relationship between their crystal morphology and electrochemical performance [34–37]. In our system, morphology-controlled preparation of different $LiCoO_2$ nanocrystals, namely polyhedrons and spheres, can be easily achieved. Although the crystal sizes of the two as-obtained samples are nearly the same, their electrochemical properties are quite different from each other. Figure 4(a) shows the first charge/discharge curves obtained from cells containing $LiCoO_2$ polyhedrons and spheres, performed at a constant rate of 140 mA/g (~1 C) between potential limits of 3.0 and 4.2 V. It can be seen from the curves that there exists much more serious polarization for the polyhedron sample compared to the sphere sample (the gap between charge and discharge curves of the former is bigger than that of the latter), indicating poorer dynamic performance of the polyhedral particle-based electrode compared to the spherical particle-based one. Figure 4(b) displays the cycle life of the two cells, from which we can see that the discharge capacity for spherical $LiCoO_2$ is some 20 mA·h/g higher than that for polyhedral $LiCoO_2$. Certainly, the electrochemical performance is also related to some other parameters such as calcination temperature and time. A detailed

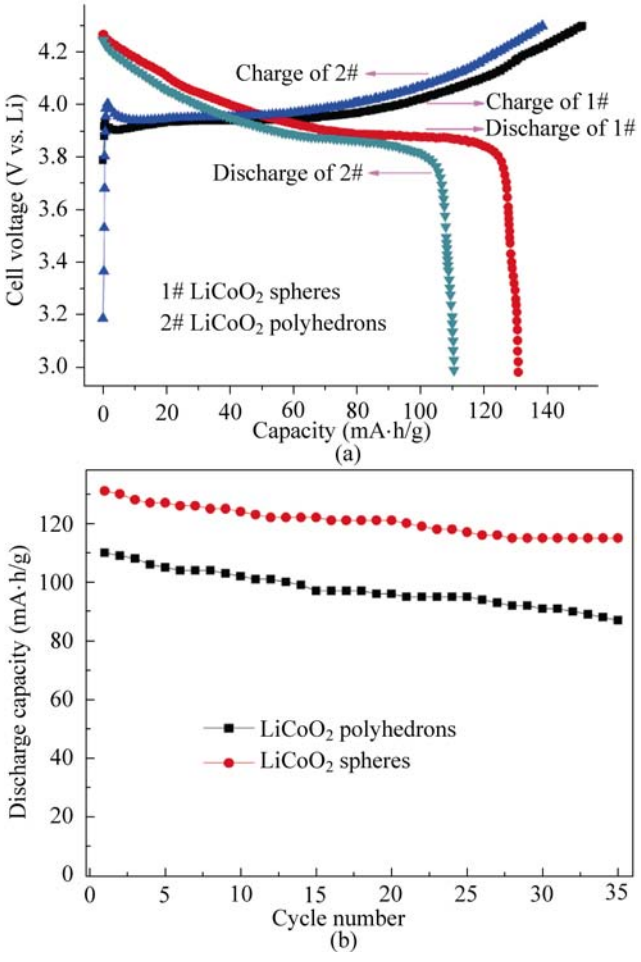

Figure 4 (a) The first charge/discharge curves obtained from cells containing $LiCoO_2$ polyhedrons and spheres. (b) The cycle life of these two cells

discussion of the behavior of lithium batteries containing as-prepared novel-shaped $LiCoO_2$ particles as electrodes will be described in a subsequent paper.

3. Conclusions

This work presents a successful morphology-controllable synthesis of CoO and $LiCoO_2$ nanocrystals. In particular, we explained the formation of CoO octahedrons exposing only high-energy (111) facets based on theoretical calculations; these should also be a useful tool for directing future face-controlled preparation of other nanocrystals. More importantly, the as-obtained two novel-shaped $LiCoO_2$ nanocrystals showed different electrochemical performance, indicating that Li-insertion/deintercalation dynamics might be crystal face-sensitive. Therefore, the preparation of other electrode nanocrystals (such as $LiCoO_2$, $LiNiO_2$, $LiMnO_2$, $LiMn_2O_4$, and $LiFePO_4$) exposing electrochemically active facets to improve their performance should be a promising direction for future studies of the application of nanoscale materials in lithium batteries.

Acknowledgements

This work was supported by the National Natural Science Foundation of China (NSFC) (No. 90606006), and the State Key Project of Fundamental Research for Nanoscience and Nanotechnology (No. 2006CB932300).

Electronic Supplementary Material: XRD patterns of CoO octahedrons and spheres and of $LiCoO_2$ polyhedrons and spheres are available in the online version of this article at http://dx.doi.org/10.1007/s12274-010-1001-9 and are accessible free of charge.

References

[1] Huang, Y.; Duan, X. F.; Wei, Q. Q.; Lieber, C. M. Directed assembly of one-dimensional nanostructures into functional networks. *Science* **2001**, *291*, 630–633.

[2] Xia, Y. N.; Yang, P. D.; Sun, Y. G.; Wu, Y. Y.; Mayers, B.; Gates, B.; Yin, Y. D.; Kim, F.; Yan, Y. Q. One-dimensional nanostructures: Synthesis, characterization, and applications. *Adv. Mater.* 2003, *15*, 353–389.

[3] Burda, C.; Chen, X.; Narayanan, R.; El-Sayed, M. A. Chemistry and properties of nanocrystals of different shapes. *Chem. Rev.* **2005**, *105*, 1025–1102.

[4] Jun, Y. W.; Choi, J. S.; Cheon, J. Shape control of semiconductor and metal oxide nanocrystals through nonhydrolytic colloidal routes. *Angew. Chem. Int. Ed.* **2006**, *45*, 3414–3439.

[5] Wang, D. S.; Xie, T.; Li, Y. D. Nanocrystals: Solution-based synthesis and applications as nanocatalysts. *Nano Res.* **2009**, *2*, 30–46.

[6] Peng, X. G.; Manna, L.; Yang, W. D.; Wickham, J.; Scher, E.; Kadavanich, A.; Alivisatos, A. P. Shape control of CdSe nanocrystals. *Nature* **2000**, *404*, 59–61.

[7] Yin, Y. D.; Alivisatos, A. P. Colloidal nanocrystal synthesis and the organic–inorganic interface. *Nature* **2005**, *437*, 664–670.

[8] Habas, S. E.; Lee, H.; Radmilovic, V.; Somorjai, G. A.; Yang, P. D. Shaping binary metal nanocrystals through epitaxial seeded growth. *Nat. Mater.* **2007**, *6*, 692–697.

[9] Viswanatha, R.; Battaglia, D. M.; Curtis, M. E.; Mishima, T. D.; Johnson, M. B.; Peng, X. G. Shape control of doped semiconductor nanocrystals (d-dots). *Nano Res.* **2008**, *1*, 138–144.

[10] Xie, T.; Li, S.; Peng, Q.; Li, Y. D. Monodisperse BaF_2 nanocrystals: Phases, size transitions, and self-assembly. *Angew. Chem. Int. Ed.* **2009**, *48*, 196–200.

[11] Zhou, K. B.; Wang, X.; Sun, X. M.; Peng, Q.; Li, Y. D. Enhanced catalytic activity of ceria nanorods from well-defined reactive crystal planes. *J. Catal.* **2005**, *229*, 206–212.

[12] Bratlie, K. M.; Lee, H.; Komvopoulos, K.; Yang, P. D.; Somorjai, G. A. Platinum nanoparticle shape effects on benzene hydrogenation selectivity. *Nano Lett.* **2007**, *7*, 3097–3101.

[13] Hu, L. H.; Peng, Q.; Li, Y. D. Selective synthesis of Co_3O_4 nanocrystal with different shape and crystal plane effect on catalytic property for methane combustion. *J. Am. Chem. Soc.* **2008**, *130*, 16136–16137.

[14] Yang, H. G.; Sun, C. H.; Qiao, S. Z.; Zou, J.; Liu, G.; Smith, S. C.; Cheng, H. M.; Lu, G. Q. Anatase TiO_2 single crystals with a large percentage of reactive facets. *Nature* **2008**, *453*, 638–641.

[15] Yin, J. S.; Wang, Z. L. Ordered self-assembling of tetrahedral oxide nanocrystals. *Phys. Rev. Lett.* **1997**, *79*, 2570–2573.

[16] Kodama, R. H. Magnetic nanoparticles. *J. Magn. Magn. Mater.* **1999**, *200*, 359–372.

[17] Xu, C.; Liu, Y. K.; Xu, G. D.; Wang, G. H. Fabrication of CoO nanorods via thermal decomposition of CoC_2O_4 precursor. *Chem. Phys. Lett.* **2002**, *366*, 567–571.

[18] Skumryev, V.; Stoyanov, S.; Zhang, Y.; Hadjipanayis, G.; Givord, D.; Nogues, J. Beating the superparamagnetic limit with exchange bias. *Nature* **2003**, *423*, 850–853.

[19] Tarascon, J. M.; Armand, M. Issues and challenges facing rechargeable lithium batteries. *Nature* **2001**, *414*, 359–367.

[20] Jiao, F.; Shaju, K. M.; Bruce, P. G. Synthesis of nanowire and mesoporous low-temperature $LiCoO_2$ by a post-templating reaction. *Angew. Chem. Int. Ed.* **2005**, *44*, 6550–6553.

[21] Li, X. X.; Cheng, F. Y.; Guo, B.; Chen, J. Template-synthesized $LiCoO_2$, $LiMn_2O_4$, and $LiNi_{0.8}Co_{0.2}O_2$ nanotubes as the cathode materials of lithium ion batteries. *J. Phys. Chem. B* **2005**, *109*, 14017–14024.

[22] Kang, K. S.; Meng, Y. S.; Bréger, J.; Grey, C. P.; Ceder, G. Electrodes with high power and high capacity for rechargeable lithium batteries. *Science* **2006**, *311*, 977–980.

[23] Seo, W. S.; Shim, J. H.; Oh, S. J.; Lee, E. K.; Hur, N. H.; Park, J. T. Phase- and size-controlled synthesis of hexagonal and cubic CoO nanocrystals. *J. Am. Chem. Soc.* **2005**, *127*, 6188–6189.

[24] An, K.; Lee, N.; Park, J.; Kim, S. C.; Hwang, Y.; Park, J. G.; Kim, J. Y.; Park, J. H.; Han, M. J.; Yu, J. J.; Hyeon, T. Synthesis, characterization, and self-assembly of pencil-shaped CoO nanorods. *J. Am. Chem. Soc.* **2006**, *128*, 9753–9760.

[25] Yang, H. M.; Ouyang, J.; Tang, A. D. Single step synthesis of high-purity CoO nanocrystals. *J. Phys. Chem. B* **2007**, *111*, 8006–8013.

[26] Wang, D. S.; Xie, T.; Peng, Q.; Zhang, S. Y.; Chen, J.; Li, Y. D. Direct thermal decomposition of metal nitrates in octadecylamine to metal oxide nanocrystals. *Chem. Eur. J.* **2008**, *14*, 2507–2513.

[27] Lagunas, A.; Payeras, A. M. I.; Hmeno, C.; Puntes, V. F.; Pericàs, M. A. Low-temperature synthesis of CoO nanoparticles via chemically assisted oxidative decarbonylation. *Chem. Mater.* **2008**, *20*, 92–100.

[28] Yin, J. S.; Wang, Z. L. *In situ* structural evolution of self-assembled oxide nanocrystals. *J. Phys. Chem. B* **1997**, *101*, 8979–8983.

[29] Ghosh, M.; Sampathkumaran, E. V.; Rao, C. N. R. Synthesis and magnetic properties of CoO nanoparticles. *Chem. Mater.* **2005**, *17*, 2348–2352.

[30] Liu, J. F.; Yin, S.; Wu, H. P.; Zeng, Y. W.; Hu, X. R.; Wang, Y. W.; Lv, G. L.; Jiang, J. Z. Wurtzite-to-rocksalt structural transformation in nanocrystalline CoO. *J. Phys. Chem. B* **2006**, *110*, 21588–21592.

[31] Zhang, Y. L.; Zhu, J.; Song, X.; Zhong, X. H. Controlling the synthesis of CoO nanocrystals with various morphologies. *J. Phys. Chem. C* **2008**, *112*, 5322–5327.

[32] Okubo, M.; Hosono, E.; Kim, J.; Enomoto, M.; Kojima, N.; Kudo, T.; Zhou, H.; Honma, I. Nanosize effect on high-rate Li-ion intercalation in $LiCoO_2$ electrode. *J. Am. Chem. Soc.* **2007**, *129*, 7444–7452.

[33] Conesa, J. C. Computer modeling of surfaces and defects on cerium dioxide. *Surf. Sci.* **1995**, *339*, 337–352.

[34] Shaju, K. M.; Bruce, P. G. Macroporous $Li(Ni_{1/3}Co_{1/3}Mn_{1/3})O_2$: A high-power and high-energy cathode for rechargeable lithium batteries. *Adv. Mater.* **2006**, *18*, 2330–2334.

[35] Kim, D. K.; Muralidharan, P.; Lee, H. W.; Ruffo, R.; Yang, Y.; Chan, C. K.; Peng, H.; Huggins, R. A.; Cui, Y. Spinel $LiMn_2O_4$ nanorods as lithium ion battery cathodes. *Nano Lett.* **2008**, *8*, 3948–3952.

[36] Li, Y. G.; Tan, B.; Wu, Y. Y. Mesoporous Co_3O_4 nanowire arrays for lithium ion batteries with high capacity and rate capability. *Nano Lett.* **2008**, *8*, 265–270.

[37] Chen, H. L.; Grey, C. P. Molten salt synthesis and high rate performance of the "desert-rose" form of $LiCoO_2$. *Adv. Mater.* **2008**, *20*, 2206–2210.